HAL
open science

When anthraquinone dyes meet pillared montmorillonite: Stability or fading upon exposure to light?

Pollyana Trigueiro, Francisco A.R. Pereira, David Guillermin, Baptiste Rigaud, Sébastien Balme, Jean-Marc Janot, Ieda M.G. dos Santos, Maria G. Fonseca, Philippe Walter, Maguy Jaber

To cite this version:

Pollyana Trigueiro, Francisco A.R. Pereira, David Guillermin, Baptiste Rigaud, Sébastien Balme, et al.. When anthraquinone dyes meet pillared montmorillonite: Stability or fading upon exposure to light?. Dyes and Pigments, 2018, 159, pp.384-394. 10.1016/j.dyepig.2018.06.046 . hal-01871692

HAL Id: hal-01871692

https://hal.umontpellier.fr/hal-01871692v1

Submitted on 18 Jan 2019

HAL is a multi-disciplinary open access archive for the deposit and dissemination of scientific research documents, whether they are published or not. The documents may come from teaching and research institutions in France or abroad, or from public or private research centers.

L'archive ouverte pluridisciplinaire **HAL**, est destinée au dépôt et à la diffusion de documents scientifiques de niveau recherche, publiés ou non, émanant des établissements d'enseignement et de recherche français ou étrangers, des laboratoires publics ou privés.

When anthraquinone dyes meet pillared montmorillonite: stability or fading upon exposure to light?

Pollyana Trigueiro[1,2], Francisco Rodrigues Pereira[1,3], David Guillemin[1], Baptiste Rigaud[4], Sebastien Balme[5], Jean-Marc Janot[5], Ieda M. G. dos Santos[6], Maria G. Fonseca[6], Philippe Walter[1], Maguy Jaber[1]*

[1]*Universités, UPMC Paris06, UMR 8220, Laboratoire d'Archéologie Moléculaire et Structurale, 4 place Jussieu, F-75005 Paris, France*

[2]*Materials Engineering Department of Universidade Federal da Paraíba, João Pessoa, Paraíba, Brazil*

[3]*Chemistry Department of Universidade Estadual da Paraíba, Campina Grande, Paraíba, Brazil*

[4]*CNRS Institut des Matériaux de Paris Centre (FR2482), 4 place jussieu, 75005 Paris, France*

[5]*Institut Européen des Membranes, UMR 5635, Université de Montpellier, ENSCM, CNRS, Place Eugène Bataillon, F-34095 Montpellier cedex 5, France*

[6]*Chemistry Department of Universidade Federal da Paraíba, João Pessoa, Paraíba, Brazil*

[7]*Materials Engineering Department of Universidade Federal do Piaui, Teresina, Piaui, Brazil*

Corresponding authors

*Maguy Jaber : maguy.jaber@upmc.fr

Abstract

Hybrid pigments have attracted great interest due to their stability and physicochemical properties that can be used in paintings, artworks and in the field of cultural heritage. The study of new materials includes the search for new pigments by immobilization of the dyes in resistant substrates such clays minerals to get new color fonts and materials with high stability. Organic-inorganic based lake pigments, at different pH, have been prepared. Ti- and Al-pillared montmorillonite were synthesized and loaded with carminic acid (CA) and alizarin (Aliz) organic dyes. The pillaring process was investigated by X-ray diffraction, textural analysis, transmission electronic microscopy and solid state nuclear magnetic resonance of ^{27}Al. The interactions between the organic guest and the inorganic host were highlighted by infrared, ^{13}C and ^{27}Al solid state magnetic nuclear resonance and time resolved fluorescence spectroscopies. The spectra support complex formation between the chromophores and the inorganic matrix. The colours of the pigments prepared were pH dependent. Lake pigments based on Al-Pillared Mt were more stable under light than Ti-based hybrid, even in oil painting formulations.

Keywords: Hybrid pigment, Pillared clay, Carminic acid, Alizarin, NMR, Fluorescence, Photoaging.

1.0 Introduction

Through centuries, paintings have represented the expression through art of some characteristics of human and social behaviour, also reflecting the impacts of environmental aspects. However, the poor stability of the colours used against acids, light or temperature has been a serious problem that has affected works of art and aspects of their cultural heritage as result of their public exposure. Thus, designs for stable pigments are desired in order to prepare/restore paintings and overcome the problem of degradation [1]. It has been expected that the surface where pigments are applied is a preponderant factor in determining the efficiency/stability of colours, and the perfection of paintings. Although there are many sources, there is a necessity to find combinations of raw materials for use as colouring agents/colourants in ink formulations. In fact, hybrid pigments have wide applications not only in works of art, but also in the fields of optics, food processing, cosmetics or plastics [2–4]. Hybrid based on organic dye-inorganic compounds are chemically obtained by a strong interaction between organic chromophores and inorganic matrices aiming to obtain stable pigments [8] or removing anionic dyes from wastewater [5]. In this context, a growing application of inorganic dyes-based hybrids are established [6–8].

Anthraquinones are classified as the natural organic dyes most resistant to light-induced deterioration used since prehistoric times [9]. These red colourants may be extracted from the roots of a diversity of plants from the Rubiaceae family (madder family). Alizarin and purpurin are the principal occurring dyes in *Rubia tinctoria L.* (maddergenus) [2,9]. Lakes are pigments formed from a dye-inorganic hybrid. Several other guest dyes have been reported in the literature to obtain lake pigments, such as carminic acid [1,8], fluorescein [8], betalain [10] and eosin [11].

Clays have attracted broad attention in the field of lake pigments because they are environment-friendly and low-cost materials and abundant in nature. Furthermore, some clay properties, such as high adsorption capacity and great potential for ion exchange, highlight their use as an inorganic support [12,13]. There are many confirmed examples of their use in clay-based lake pigments throughout history. A well-known example is “Maya Blue” which is a combination of indigo derived from the leaves of the local *añil* plant (*Indigofera suffruticosa*) with palygosrskite, a clay mineral of fibrous nature found in the Yucatán Peninsula [14]. The hybrid compound has conserved a strong blue colour in Mayan artworks up to this day. Recently, it has been some papers have reported clay-based lake pigments such as Maya Blue-like [15], acid-activated sepiolite/Rhodamine B@SiO_2 fluorescent pigments [16], Halloysite/$CoAl_2O_4$ hybrid pigments [7], Attapulgite/Fe (III) hybrid red pigments [3], Fe_2O_3 supported on sepiolite or halloysite [17], Carminic acid onto montmorillonite [1].

Among clay minerals, montmorillonite has attracted remarkable attention in the field of lake-based hybrids due to its peculiar features, such as swelling with a larger lamellar expansion capacity in aqueous solution. Moreover, its surface area negatively charged in an acid medium, enables it to interact with bulky molecules, such as cationic dyes [1,18]. Montmorillonite is a 2:1 type clay mineral, member of smectite group, with a hydrous layered aluminium silicate with a high cationic exchange capability (CEC) and active hydroxyl groups [19]. Its layers consist of two tetrahedral silica sheets sandwiching one octahedral aluminium sheet. The cationic layered clays can be transformed into highly porous structures by a process known as pillarization. Pillaring provides chemical and thermal stability to clays as well as increasing interlayer space and surface area [20,21]. The most common type of pillared clays is obtained by the incorporation of aluminium polyhydroxylations in the interlayer space of the clay, calcination is essential to ensure the formation of nanoscale

alumina particles in the material [20,21]. Additionally, many other polycations formed upon hydrolysis of Zr^{4+}, Ti^{4+}, Cr^{3+}, Fe^{3+} or Ga^{3+} were reported for pillaring clays [21,22].

In this perspective, the present investigation aimed to synthesize Ti- and Al-pillared montmorillonite and evaluate their influences on the photostability of new lake pigments and oil painting formulations. Alizarin (1,2-dihydroxyanthraquinone) and carminic acid (7-C-α-glucopyranosyl-3,5,6,8-tetrahydroxy-1-methyl-2-anthraquinone carboxylic acid) were used as dyeing agents.

2.0 EXPERIMENTAL

All chemicals applied in this work were purchased from Aldrich or Sigma-Aldrich with an analytical grade and used without any previous purification.

2.1 Montmorillonite (Mt) synthesis

The reagents were mixed in the following order: deionized water, hydrofluoric acid and the sources of interlamellar cation sodium acetate, magnesium acetate, alumina and silica. The hydrogel with the molar composition of $SiO_2.0.2Al_2O_3.0.4MgO.0.05Na_2O.xH_2O$ was aged under stirring at room temperature for 2 h and then was autoclaved at 220 °C for 72 h [19,23]. The autoclaves were cooled to room temperature and the product were washed thoroughly with distilled water and centrifuged. Finally, the obtained Mt was dried at 50 °C for 72 h.

2.2 Pillaring process of Montmorillonite (PILC)

The procedures for the pillaring process of Mt with aluminium polyhydroxycations and titanium ions followed the procedures adapted from Bergaoui et al [24] and Tomul et al [25], respectively.

For aluminium, the pillaring solution was obtained by hydrolysis of aluminium chloride with a NaOH solution up to OH:Al ratio of 2.2 and final concentration of 0.1 mol.L^{-1}. This mixture was left to stand for 24 h at room temperature under stirring. Meanwhile, 3.2 g.L^{-1} of the aqueous clay suspension (7.3 mmol Al^{3+}.g clay) was aged under stirring at room temperature for 3 h. Then, aluminium solution was added dropwise to a clay suspension with flow of 1 mL.min^{-1}. The resulting solution was stirred 24 h at room temperature, washed and dried at 50 °C for 24 h. The samples upon aluminium cations intercalation were denoted Al-Mt. The samples were calcined up to 500 °C for 2 h. The pillared clay samples with aluminium cations were denoted PILC-Al.

For titanium, the pillaring solution was prepared by hydrolysis of titanium isopropoxide with 6 M HCl solution with Ti^{4+}:H^{+} molar ratio at 1:4. Titanium source solution was added dropwise with flow of 0.4 mL.min^{-1} and the result solution was left stirring at room temperature for 6 h. Then, deionized water was added until reaching a concentration of 1 M H^{+} and 0.25 M Ti^{4+}. The pillaring solution was introduced dropwise with a flow of 1 mL.min^{-1} to the Mt suspension until to reach 10 mmol Ti^{4+}.g clay. The resulting suspension was stirred for 24 h at room temperature and then washed with deionized water until total chloride removal. The prepared solid was recovered by centrifugation and dried at 50 °C for 24 h. Samples upon titanium cations intercalation were denoted Ti-Mt. The samples were calcined up to 400 °C for 2 h. Pillared clay samples with titanium cations were denominated as PILC-Ti.

2.3 Dyeing procedure

Pillared montmorillonite was loaded with alizarin (Aliz) and carminic acid (CA) considering the different values of pK_a. It is known that carminic acid presents three different values of

pK_a (2.8, 5.4 and 8.1) [1,26], while alizarin has only two values (6.6 - 7.5 and 12.4 - 13.5) [9,27].

For each sample, 300 mg of pillared montmorillonite was added to 100 mL of carminic acid (0.6 $g.L^{-1}$) or alizarin (0.8 $g.L^{-1}$) solution and was left under stirring for 4 h. The samples were then centrifugated, washed with deionized water and dried at 50 °C for 24 h.

2.4 Oil painting formulation

All the formulations were obtained by incorporating 35 mg of pigment in 400 µL of linseed oil. The mixture was then grinded and an homogeneous paste is obtained. Films were then prepared on slice glasses using specific applicator. Linseed oil is one of the earliest and the most commonly vehicle applied to ink formulations that remains been used nowadays.

3.0 CHARACTERIZATIONS

3.1 X-ray diffraction (XRD)

Powder X-ray diffractograms were recorded using D8 Advance Bruker-AXS Powder X-ray diffractometer with CuK_α radiation (λ= 1.5405 Å). XRD patterns were performed between 5-70° (2θ) with scan rate of 0.5 $deg.min^{-1}$. The active area of the detector was limited as much as possible in order to reduce the background scattering at low angle between 2-10° (2θ).

3.2 Textural investigation

Nitrogen adsorption-desorption isotherms were measured at liquid nitrogen temperature on a Micromeritics ASAP 2020 apparatus. The specific surface area (S_{BET}) was evaluated using the Brunauer-Emmett-Teller (BET) method. The pore size distribution was determined from the desorption part of the isotherm using the Barret-Joyner-Halender (BJH) method [28].

3.3 Transmission electron microscopy (TEM)

TEM study of the samples was performed on a JEOL 2010 microscope, 200 kV LaB_6 coupled Orius camera, from Gatan Company. Samples in the form of bulk powders were suspended in ethanol and then deposited on 400 mesh copper grids covered with an ultrathin carbon membrane of 2 – 3 nm thickness.

3.4 ATR-FTIR

Infrared analyzes was performed on Agilent Cary 630 FTIR spectrometer using Agilent diamond Attenuated Total Reflectance (ATR) technique mode, being spectral resolution > 2 cm^{-1} and 32 scans. Spectra were acquired by Microlab FTIR Software (Agilent Technologies). Spectra were acquired between 4000 and 650 cm^{-1}.

3.5 Thermal Analysis (TG/DTG)

Thermogravimetric analyses were carried out using a TA Instrument SDT Q600 analyzer. The heating rate was of 5 °C.min from 25 °C to 800 °C, under dry air flow of 10 mL.min, and using alumina pan.

3.6 Solid state nuclear magnetic resonance (^{13}C CP-MAS and ^{27}Al MAS-NMR)

^{13}C and ^{27}Al MAS NMR spectra were obtained on a Bruker Avance III spectrometer equipped with a 4 mm H-X MAS probe, operating at frequency of 500.17 MHz (^{1}H), 125.77 MHz (^{13}C) and 130.33 MHZ (^{27}Al). Chemical shifts were calibrated using the carboxyl signal of adamantane (38.52 ppm) for ^{13}C and $AlNO_3$ (O ppm) for ^{27}Al as external standard.

The ^{13}C Cross-Polarization spectra were acquired with a MAS rate of 14 kHz, a ramp-CP contact time of 1 ms and a 1 s recycle delay and with a ^{1}H decoupling spinal. Over an acquisition time of 40 ms, the number of scans to obtain the spectra depends on the S/N obtained for each sample. Spectra were processed with a zero-filling factor of 2 and with an

exponential decay corresponding to a 25 Hz line broadening in the transformed spectra. Only spectra with the same line broadening are directly compared.

The ^{27}Al experiment using 30° pulse is recorded in the same condition of spinning rate, 100 kHz spectral width and with 500 ms recycle delay.

3.7 Fluorescence Characterisation

Time-resolved fluorescence spectroscopy was obtained by the time-correlated single-photon counting technique on lab-made device previously described [23,29]. For the analysis the fluorescence decay law at the magic angle $I_M(t)$ were analyzed as a sum of exponentials:

$$I_M(t) = \frac{1}{3}\sum_{i=1}^{n} \alpha_i \, e^{-t/\tau_i} \qquad \text{(eq 1)}$$

Where, τ_i is the fluorescence lifetime and α_i is the pre-exponential factor related to the contribution of each lifetime of the component *i*.

Fluorescence lifetimes were calculated from data collected at magic angle by iterative adjustment after convolution of a pump profile (scattered light) with a sum of exponentials as described previously. The criteria to evaluate the quality of fit are χ^2 the and the residue function. The fluorescent decay was recorded at λ_{em}=600 nm under excitation λ_{ex}=540 nm or λ_{em}=550 nm for carminic acid and alizarin, respectively.

3.8 Light-Induced Aging

Aging effects were simulated by exposure of solid pigments and oil paint formulations to white light irradiation for 340 hours, using a LED lamp set to provide 50 Klx of illumination intensity.

Spectrophotocolorimetry was performed using an Ocean Optics Halogen and Deuterium Light Source HL-2000-FHSA device as incident light beam and ocean optics USB4000 detector for

acquisition. Ocean Optics QP400-1-UV-VIS fiberglass was used to link these devices. For each acquisition, an average of 100 scans were useful to obtain the optimum signal. The reflectance wavelength range was set from 400 to 950 nm and measurements are done on pressed pellets samples as function of L^*, a^* and b^* coordinates. The differences of colours between unexposed and exposed samples were calculated by $\sqrt{((\Delta L^*)^2 + (\Delta a^*)^2 + (\Delta b^*)^2)}$ equation, according to the "Commission Internationale of l'Eclairage" (CIE).

4.0 RESULTS AND DISCUSSIONS

4.1 Structural and textural properties

X-ray diffraction patterns of the raw Mt and pillared-Mt samples are depicted in Figure 1a-b. Characteristic peaks of the pristine clay were observed as reported previously [30]. The d_{001} of the later is about 1.3 nm typical of one hydrated layer for Na-Mt. For PILC-A, *d* value increases from 1.3 nm to 1.64 nm suggesting an intercalation of the aluminium cations into the interlayer space of Mt. Upon calcination, the d_{001} value reached 1.75 nm due to the formation of oxide pillars as already reported [31,32].

In the case of titanium cations, the d_{001} value varies from 1.3 nm to 1.45 nm (Figure 1b, insert) due to the increase of the interlayer space upon intercalation of titanium cations in Mt. After calcination, the (001) reflexion can not be observed anymore suggesting an heterogeneous stacking of the layer in the titanium pillared Mt samples [25,33] or an exfoliation. A peak at 2θ=25.36 characteristic of anatase (TiO_2) was observed as reported previously in Ti-pillared clay minerals [34–36].

After loading with dyes, no significant changes in the d_{001} values were found in the composite materials based on pillared-Mt and dyes.

It is known that modification of clays by pillarization with metal oxides also causes the increase of the specific area and promotes a permanent mesoporosity [37–39].

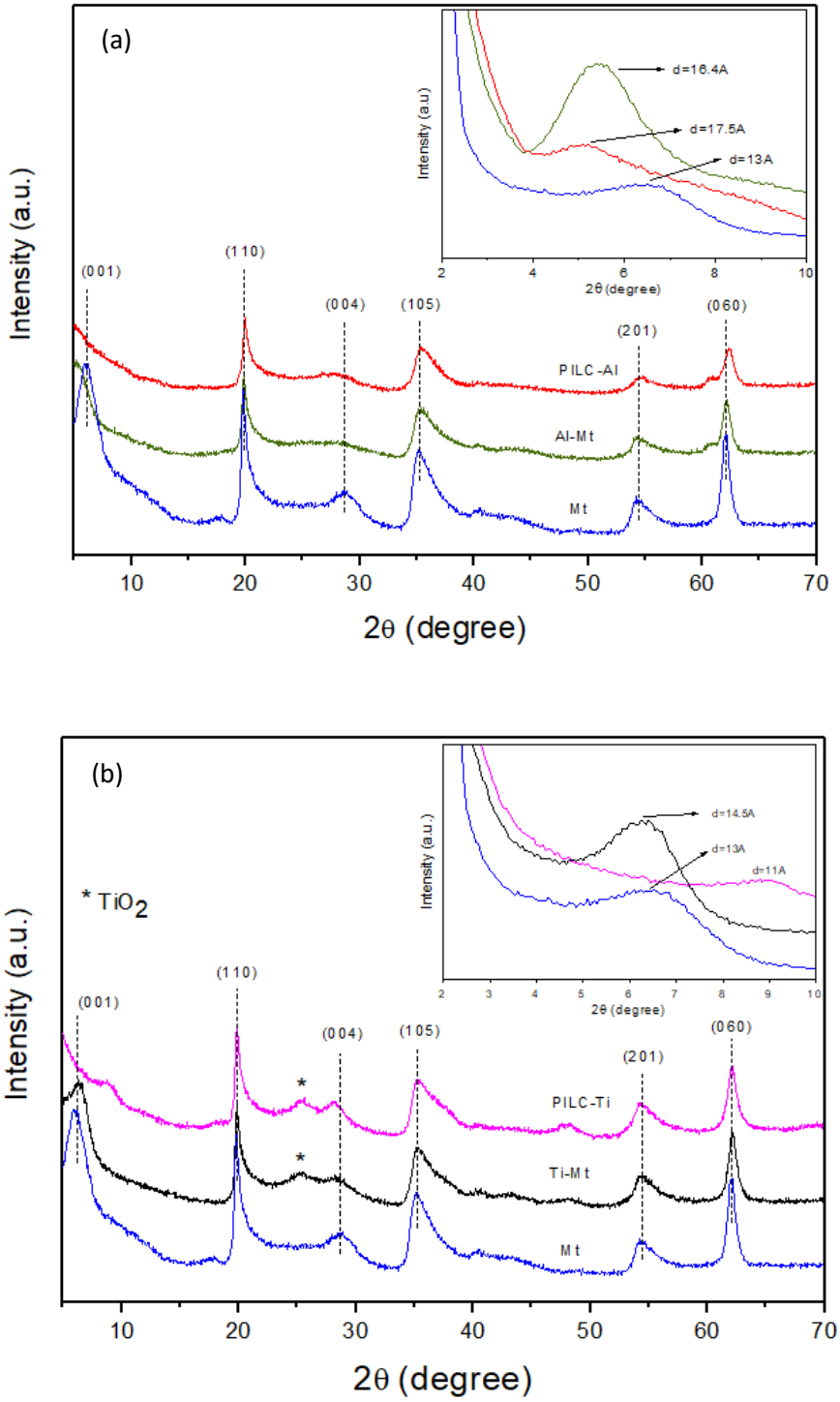

Figure 1. XRD patterns of pillared-Mt with (a) aluminium and (b) titanium cations, showing in insert the shift in the d_{001} peak upon metallic cations intercalation and upon calcination of the samples.

The N_2-adsorption/desorption isotherms and pore size distribution of the pillared clays are presented in Figure 2a and 2b. The adsorption isotherms of the pillared samples fit the Type IV, for low relative pressures, the curve is characterized by a saturation step and presence of a hysteresis loop of type H_4 [34]. This kind of adsorption isotherm is typical of mesoporous materials [35]. The multipoint BET surface area (S_{BET}) values were determined from isotherm data in the P/P_0 0.09-0.5 range. The raw clay reached a surface area of 106 $m^2.g^{-1}$, while PILC-Al and PILC-Ti exhibited values of 186 $m^2.g^{-1}$ and 204 $m^2.g^{-1}$, respectively. A narrow size distribution of the mesopores obtained by BJH method showed a diameter range between 3-5 nm and 3-6 nm for the PILC-Al and PILC-Ti samples, respectively (Figure 2b). These results suggested that the pillaring process succeed in the PILC-Al and PILC-Ti samples.

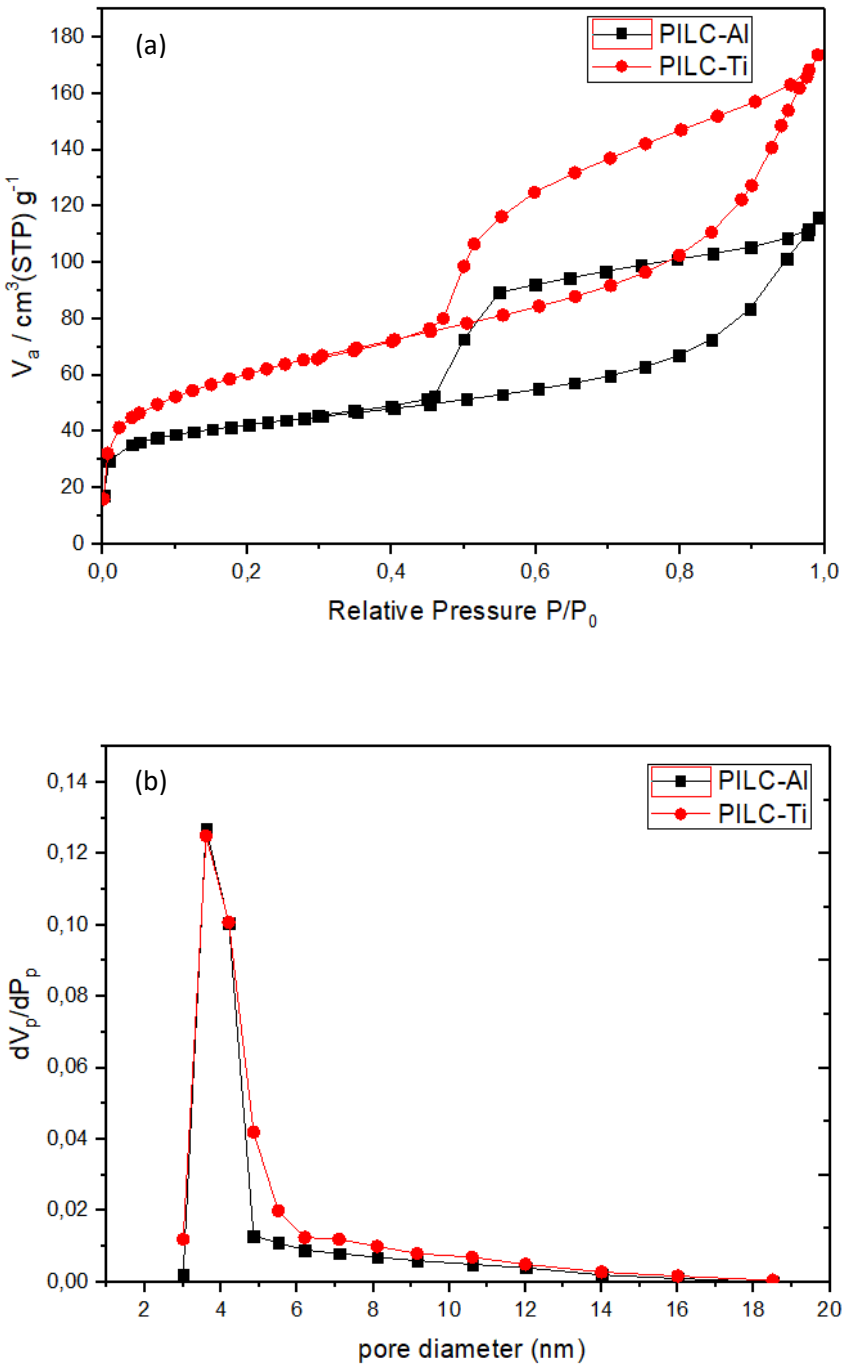

Figure 2. (a) N_2 isotherms of adsorption/desorption at 77 K and (b) pore diameter (d_p) distribution for PILC-Al and PILC-Ti samples.

4.2 Morphological analysis

TEM experiments were performed to have a better view of the intercalation of the metal cations in the interlayer of montmorillonite. TEM images of Mt shows layered structures with alternate dark and bright fringes with a calculated interlayer distance of 1.26 nm for the raw sample. It was noticed that the distance increased to 1.75 nm and about 1.4-1.8 nm for PILC-Al and PILC-Ti samples, respectively (Figure 3a-b). The results suggested that the pillaring process occurs and that the lamellar structure of Mt was maintained for both samples, in agreement with the XRD results.

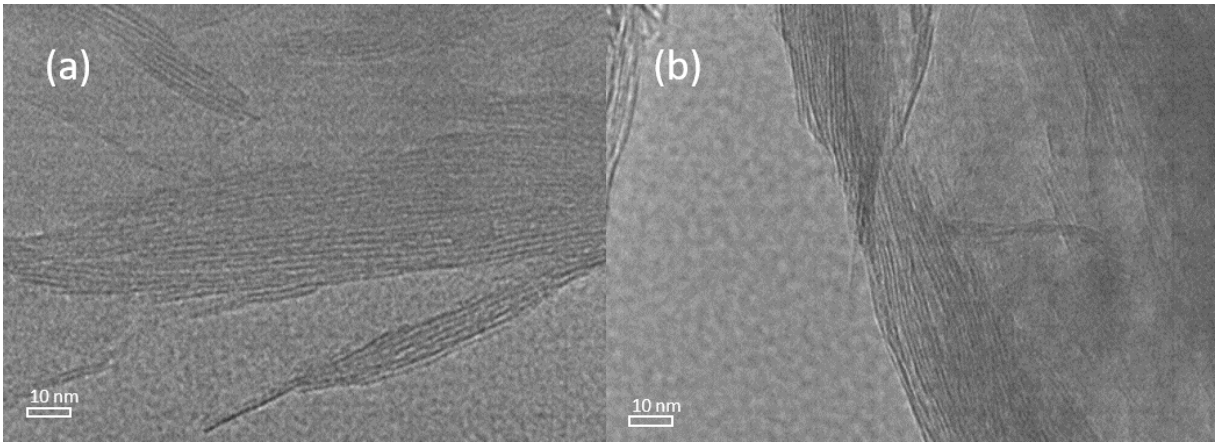

Figure 3. TEM images of (a) PILC-Al and (b) PILC-Ti samples.

4.3 ATR-Infrared

ATR-IR spectra of the pillared clay samples before and after adsorption of carminic acid and alizarin dyes are shown in Figure 4a-b. It can be noticed several characteristic bands of the dyes related to anthraquinone groups. Spectrum of bulk CA (Figure 4a) showed bands at 1611 cm^{-1}, 1563 cm^{-1} and 1428 cm^{-1} corresponding to the stretching vibration of υ(C=O) quinone group, stretching vibration of υ(C=C) aromatic and bending vibration of δ(OH) group, respectively. Bulk Aliz (Figure 4b) spectrum shows bands at 1663 cm^{-1}, 1587 cm^{-1} and 1453 cm^{-1} corresponding to the stretching vibration of υ(C=O) quinone group, stretching vibration of υ(C=C) aromatic and bending vibration to δ(OH) group, respectively [8]. Spectra of hybrid pigments with CA present shifts for some bands, in Figure 4a, the band of C=C structure

shifts from 1563 to 1558 cm^{-1} in PILC-Al-CA-pH2.5 and to 1566 cm^{-1} in PILC-Ti-CA-pH2.5. For the C=O function the band disappeared upon adsorption, the band corresponding to OH group is shifted from 1428 to 1440 cm^{-1} in PILC-Al-CA-pH2.5 and to 1442 cm^{-1} in PILC-Ti-CA-pH2.5. In the case of hybrid pigments with Aliz, in Figure 4b, the band assigned to the stretching vibration C=C aromatic shifts from 1587 to 1590 cm^{-1} for PILC-Al-Aliz-pH8.4 and to 1591 cm^{-1} in PILC-Ti-Aliz-pH8.4, the band corresponding to C=O group presented similar behaviour as CA, the band is not observed upon adsorption on clay. Finally, the band corresponding to bending vibration OH shift from 1453 to 1468 cm^{-1} for PILC-Al-Aliz-pH8.4 and to 1466 cm^{-1} in PILC-Ti-Aliz-pH8.4. These results indicate that the coordinated bonds between anthraquinone groups and modified clay minerals can occur by chelation of Al^{3+} and Ti^{4+} cations of the pillars with the quinone and catechol functions of the dyes as well as by adsorption of the dyes onto external and internal surface of clay mineral.

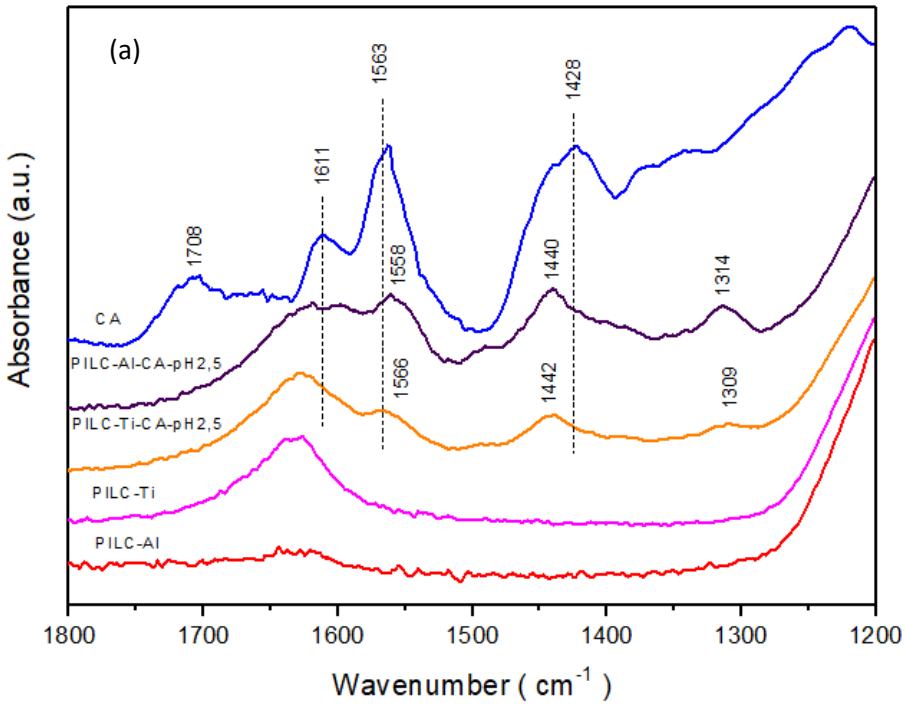

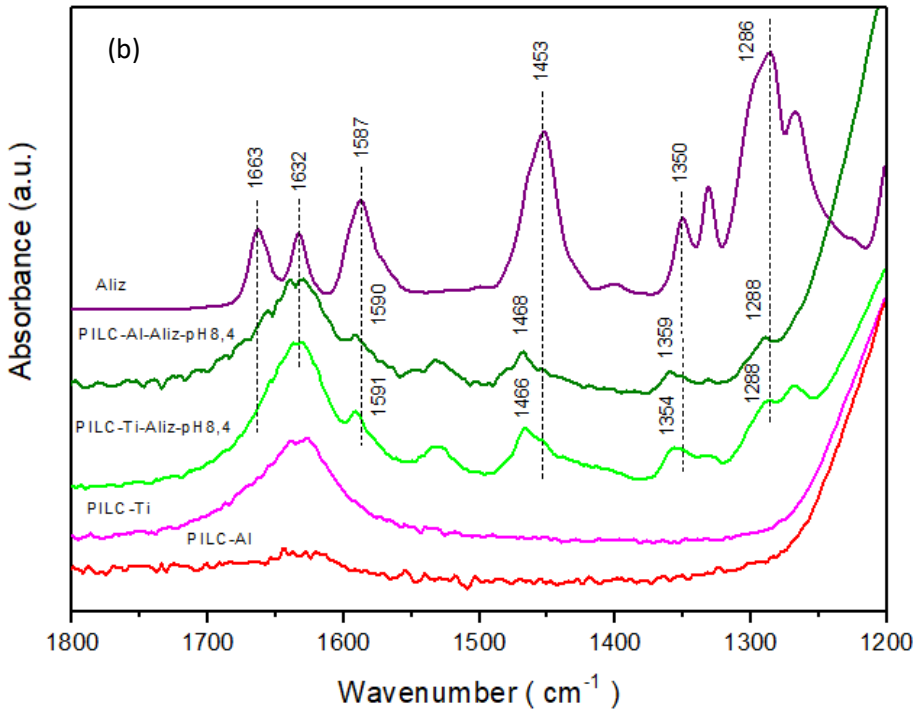

Figure 4. ATR-IR spectra of pillared clays and dyed clays with (a) carminic acid and (b) alizarin.

Thermal Analyses

DTG curves for all samples are depicted in Figure 5. The characteristic stages of the mass loss of water, organic matter and dehydroxylation, before and after adsorption of CA and Aliz dyes are shown.

Two regions of mass loss have been noticed for the raw Mt and pillared clays samples. The first one, with an endothermal event, with weight loss about 4.3-5 % at T_{max}=45 ^{o}C is attributed to the departure of physisorbed water. The second at T_{max}=630 ^{o}C, with an endothermal event, is attributed to structural dehydroxylation of the clay matrix with mass loss about 2.0 % for both samples [40].

After the dyeing process, the first peak corresponds to the dehydration with an amount between 6.5-8 %. The second peak between 350 and 560 °C for all samples corresponds to the oxidation of the organic matter. PILC-Ti dyed clays has 3.2 % of weight loss corresponding to alizarin dye and 3.5 % of carminic acid dye decomposition. PILC-Al dyed clays presents about 7.8 % of alizarin dye and 6.5 % of carminic acid dye decomposition. All the samples still show the peak related to dehydroxylation with a weight loss between 1.5-2.2 %.

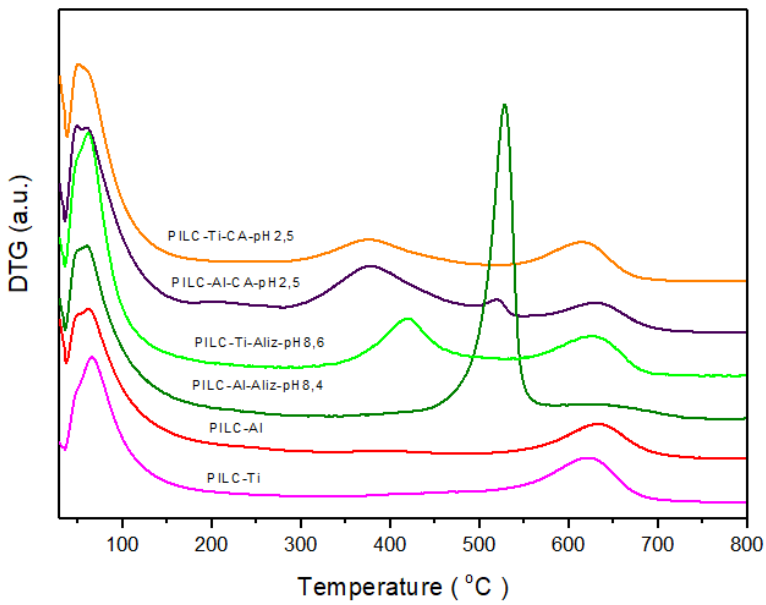

Figure 5. DTG curves for PILC-T, PILC-A, PILC-A-Aliz-pH8.6, PILC-T-Aliz-pH8.4, PILC-A-CA-pH2.5 and PILC-T-CA-pH2.5 dyed samples.

4.5 Solid state nuclear magnetic resonance of ^{13}C and ^{27}Al

^{27}Al MAS NMR spectra of PILC-Al before and after adsorption of CA and Aliz dyes are depicted in Figure 6. PILC-Al sample presented three characteristic chemical shifts at 3.4 ppm, 59.6 ppm and 28.6 ppm related to hexa-coordinated-Al (Al VI), tetra-coordinated-Al (Al IV) and penta-coordinated-Al (Al V), respectively. The intense peak of Al (VI) corresponds to the Al in the pillars and the Al (IV) signals are resulted of a overlap of the central Al in Al_{13} (Keggin structure with a tetrahedral Al atom in the centre of the cluster coordinated to 4 oxygen atoms) and small amount of Al in the tetrahedral sheets [24]. It has been noticed a shift from 3.4 to 3.3 ppm and from 3.4 to 3.2 ppm for PILC-Al-Aliz-pH8.4 and PILC-Al-CA-pH2.5 dyed samples, respectively. This may suggest the interactions between Aliz or CA and Si-OH-Al-OH in the Mt edges well as with pillars formation.

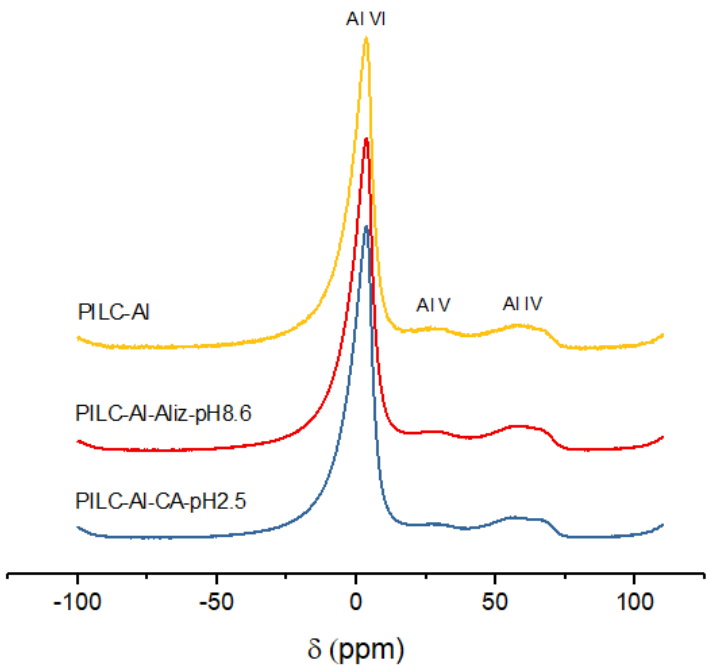

Figure 6. ^{27}Al MAS NMR of PILC-Al before and after adsorption of CA and Aliz dyes.

^{13}C MAS NMR spectra of the Al and Ti-pillared clay samples after adsorption with CA are presented in the Figure 7a. Although the spectra of the CA onto pillared clays composites exhibited almost the same signals than the raw dye, it was observed some changes in the chemical shifts. In bulk CA, the signal at 20.9 ppm is related to methyl group of C8 and the region between 60-80 ppm is attributed to the sugar part of the dye molecule. The signals at 171.3 ppm and 185 ppm are assigned to the carboxylate moieties and to the ketones functions, respectively [1]. Some other shifts have been observed, upon complexation, such as from 147.5 ppm to 149.2 ppm and 148.3 ppm, attributed to C4 signal for PILC-Al-CA-pH2.5 sample and PILC-Ti-CA-pH2.5, respectively. The C5 signal is shifted from 112.5 to 115.2 ppm and 114.1 ppm to PILC-Al-CA-pH2.5 and PILC-Ti-CA-pH2.5, respectively. In the region of the C9,10 the signal is not well defined for PILC-Al-CA-pH2.5 and is shifted from 185 to 186.7 ppm for PILC-Ti-CA-pH2.5. This may suggest the chelation between the metallic cations and anthraquinone groups in the dyes. Indeed, dye may also be adsorbed in clay surface. The chromophore groups in anthraquinone dyes can also behave as binding functions between the dye molecule and the mineral support through an intermediate metal atom [9].

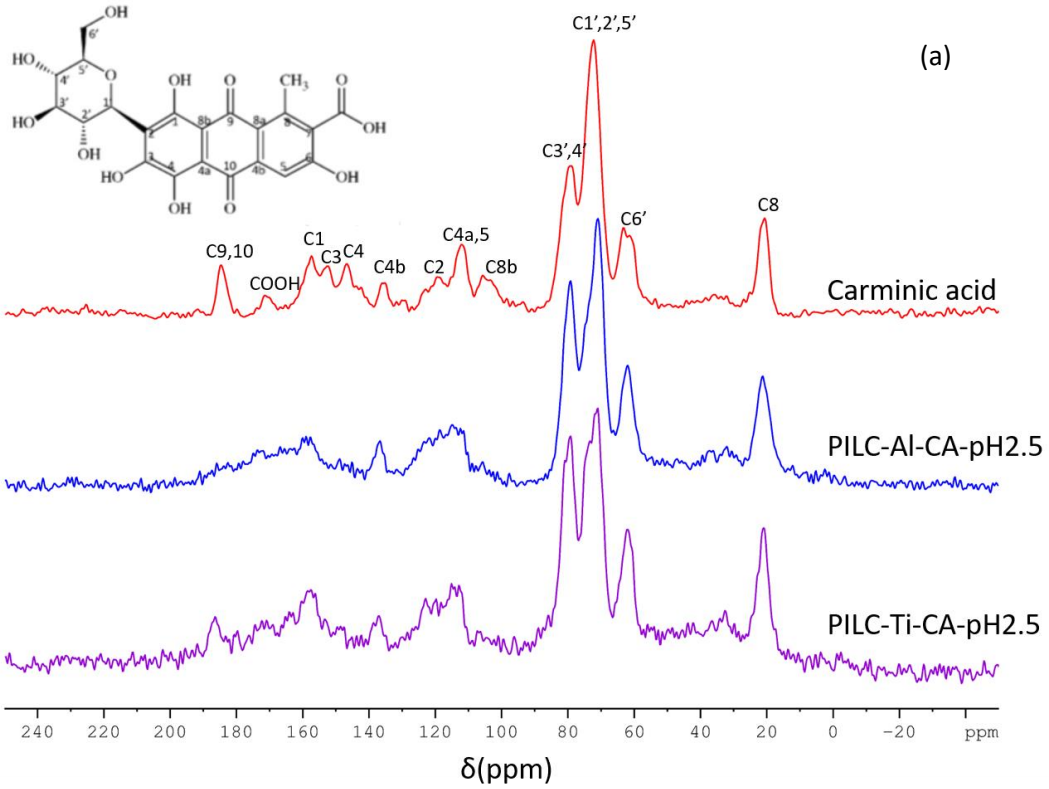

332

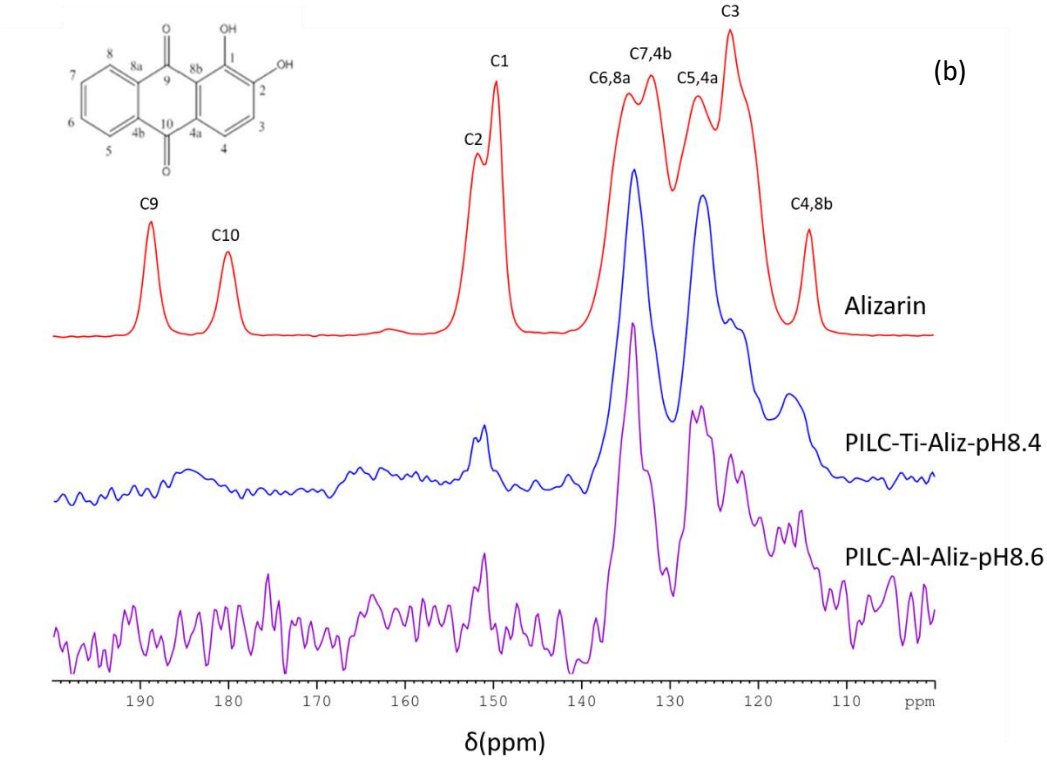

333

334 Figure 7. ^{13}C MAS NMR spectra of Al and Ti-pillared clays and dyed clays with (a) carminic acid and (b)
335 alizarin.

336

^{13}C MAS NMR spectra of the Al and Ti-pillared clay samples after adsorption with Aliz are presented in the Figure 7b. Alizarin has distinct region for the resonances of the anthraquinone partial structure and hydroxy groups. The peaks corresponding to C1 and C2, that are assigned to hydroxyl groups, are shifted from 150 and 151.8 ppm to one signal at 151.2 ppm and 151.4 ppm to PILC-Ti-Aliz-pH8.4 and PILC-Al-Aliz-pH8.6, respectively. It was notice that the signals assigned to C9 and C10 corresponding to ketone functions shifts to shoulder not well defined at approximately 184 ppm in both pillared clays. The results suggested that the ketone and hydroxyl groups of the dyes can be main attachment site with the modified inorganic matrix [41,42].

4.6 Fluorescence analysis

The time resolved fluorescence characterisation of carminic acid and alizarin free in solution and loaded on pillared clay were performed under wavelength excitation 540 nm and 550 nm respectively (Figure 8). Free in solution, the average fluorescence lifetimes are 0.151 ns and 0.596 ns for carminic acid and alizarin, respectively. They significantly increase after adsorption on pillared clay (tables I and II). This result confirms a stabilisation of both dyes due to their interactions with the clay as shown by NMR.

The fluorescence decay of the alizarin free in solution and adsorbed on all materials requires three components to be fitted. For the PILC-Ti, similar results were obtained at pH 7.1 and 3.4 suggesting similar interactions between the dye and the pillared clay. On the contrary, for PILC-Al the pH influences the fluorescence lifetime and thus the interaction are not the same, due different degrees of protonation of the molecule in these pH. The different lifetimes at pH around 7-8 for PILC-Ti and PILC-Al dyed with Alizarin confirms that the cation (Al or Ti) is involved in the interaction material/dyes.

For the carminic acid, the fluorescence results are quite different. In solution, the fluorescence decay is composed by three lifetimes (0.496 ns, 0.099 ns, and 0.048 ns). After loading on pillared clays, it requires four components among them one component longer than 1.5 ns appears. It also depends on the metal cations used for the pillaring process confirming its role in the material/dye interaction. Moreover, the degree of protonation influences the fluorescence emission properties. Indeed, for PILC-Ti-pH5 the average lifetime is 0.945 ns and the longer component represents 25.6 % of the global decay while for PILC-Ti-pH2.5 the average lifetime is shorter (0. 469 ns) and the longer component 1.723 ns represents less than 10 %. At pH 5, the carboxyl group is deprotonated and thus can be coordinated with aluminium by electrostatic interactions. On the contrary at pH 2.5 the carminic acid is totally protonated and thus the complexation with aluminium likely involved the anthraquinone and/or clay surface as suggested by NMR study.

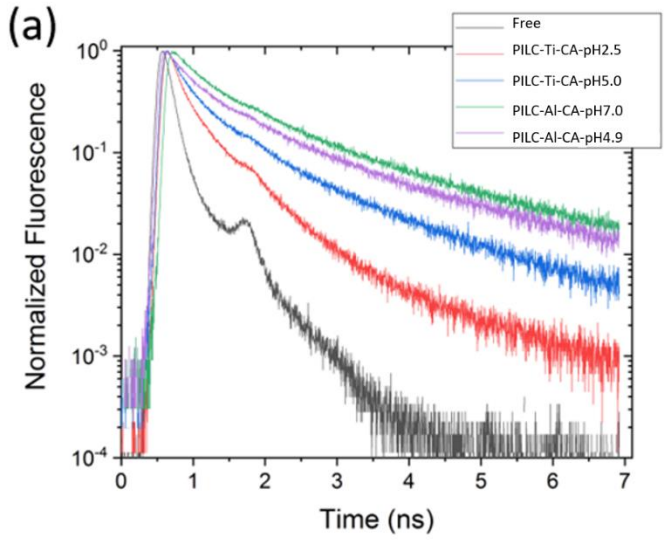

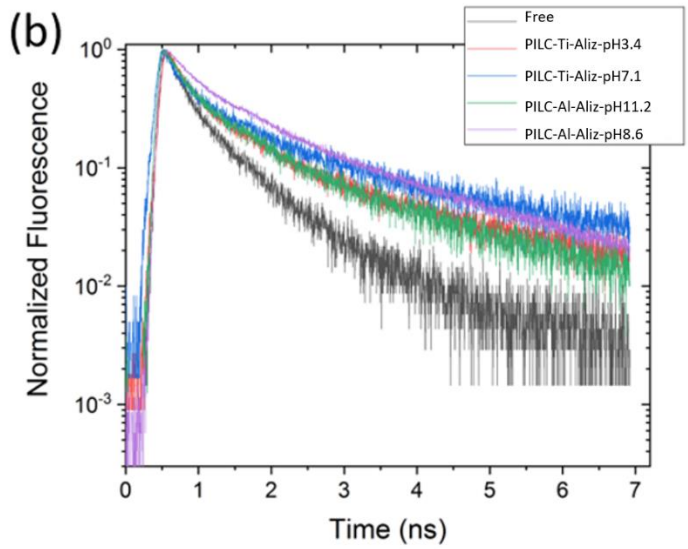

Figure 8: Fluorescence decays of carminic acid (a) and alizarin (b) free in solution and loaded on different pillared clays.

Table I: Fluorescent lifetime (τ_i) and average lifetime (τ_{AV}) results for carminic acid free in solution and loaded on pillared clay for excitation wavelength 540 nm at emission wavelength 600nm (λ_e) Yield = $100\alpha_i\tau_i/\Sigma\alpha_i\tau_i$ represents the contribution of each emission to the total emission

Samples	**τ_1 (ns) / (yield)**	**τ_2 (ns) / (yield)**	**τ_3 (ns) / (yield)**	**τ_4(ns) / (yield)**	**$\tau_{(av)}$ (ns)**	**χ^2**
CA-H_2O	0.496 *(15.9%)*	0.099 *(62.7%)*	0.048 *(21.4)*	-	0.151	0.87
PILC-Ti-CA-pH5	2.202 *(25.6%)*	0.774 *(40%)*	0.270 *(24.6%)*	0.059 *(9.9%)*	0.945	1.08
PILC-Ti-CA-pH2.5	1.723 *(9.6%)*	0.496 *(53.2%)*	0.147 *(22.2%)*	0.047 *(15%)*	0.469	1.00
PILC-Al-CA-pH4.9	2.798 *(33.7%)*	0.981 *(41.8%)*	0.326 *(20.5%)*	0.053 *(4.1%)*	1.421	1.02
PILC-Al-CA-pH7	2.91 *(37.3%)*	1.014 *(43.9%)*	0.322 *(16.1%)*	0.048 *(2.6%)*	1.584	0.99

Table II: Fluorescent lifetime (τ_i) and average lifetime (τ_{AV}) results for alizarin free in solution and loaded on pillared clay for excitation wavelength 540 nm at emission wavelength 600nm (λ_e) Yield = $100\alpha_i\tau_i/\Sigma\alpha_i\tau_i$ represents the contribution of each emission to the total emission

Samples	**τ_1 (ns) / (yield)**	**τ_2 (ns) / (yield)**	**τ_3 (ns) / (yield)**	**$\tau_{(av)}$ (ns)**	**χ^2**
Aliz-H_2O	1.094 *(37.7%)*	0.359 *(49.1%)*	0.059 *(13.2%)*	0.596	0.84

PILC-Al-Aliz-pH11.2	2.315 *(45.3%)*	0.585 *(42.5%)*	0.125 *(12.2%)*	1.313	1.09
PILC-Al-Aliz-pH8.4	2.78 *(48.5%)*	0.846 *(41.7%)*	0.189 *(9.8%)*	1.721	1.00
PILC-Ti-Aliz-pH3.4	3.217 *(42.2%)*	0.713 *(39.5%)*	0.183 *(18.2%)*	1.674	1.26
PILC-Ti-Aliz-pH7.1	3.372 *(54.5%)*	0.749 *(32.6%)*	0.183 *(12.9%)*	2.105	1.30

4.7 Colours and hue of pigments

The colours and hue variation of the pillared samples upon CA and Aliz adsorption were pH dependent (Figure 9). It is known that carminic acid presents three different values of pK_a (2.8, 5.4 and 8.1) and alizarin has two different values (6.6-7.5 and 12.4-13.5). In solution, Aliz occurs in the form of partially dissociated yellow molecules at pH below 5.2. At pH 6-10 it is deprotonated and occurs in red monovalent cations. Finally, it occurs in the violet di-anionic form at pH about 12 [43]. In turn, CA is present, in acid pH, in the orange monoanionic form. Indeed, CA bears one negative charge at pH about 4 and is entirely negative in neutral medium [1]. At pH 8, it is completely deprotonated and is present, in solution, in the violet colour tri-anionic molecule. From these observations, at low values of pH the interactions between organic dyes and clay surface is globally driven by electrostatic forces. Whereas at higher values of pH the interactions can occur through complexation of the catechol and hydroxy-keto groups of chromophore structures with the metallic cations of the pillars present in the interlamellar spaces of montmorillonite. Furthermore, it is also known that intensity of colours is dependent of the amount of the adsorbed organic dye.

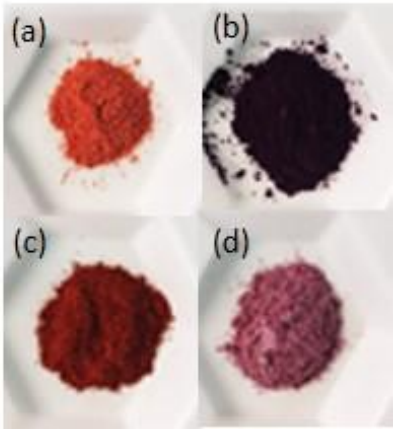

Figure 9. Colours of pigments obtained at different pH for organic dyes onto modified clay (a) PILC-A-Aliz-pH11.2; (b) PILC-A-CA-pH2.5; (c) PILC-T-Aliz-pH8.4 and (d) PILC-T-CA-pH8.0.

4.8 Light-Induced Aging

Light can be essential for appreciation of artworks, but in long time it may induces deterioration to paintings or other artefacts, causing irreversible damage which may include colour fading. Light exposure causes photooxidative degradation resulting in the breakdown of the dye molecules [44]. Then, the colours of solid pigments and oil painting prepared were evaluated before and after light exposure during 340 hours, where this time is equivalent to approximately 28 years of exposure in a museum (Figure 10a-b).

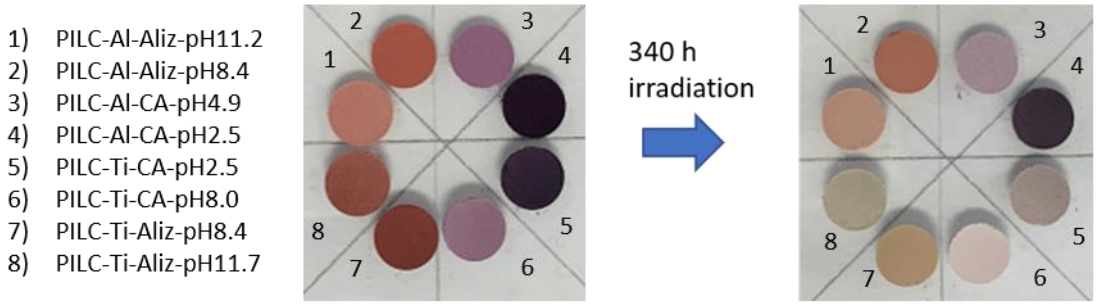

Figure 10(a). Solid pigments samples before and after LED irradiation based Aliz and CA dyes adsorbed onto Al-pillared clay (top) and Ti-pillared clay (bottom).

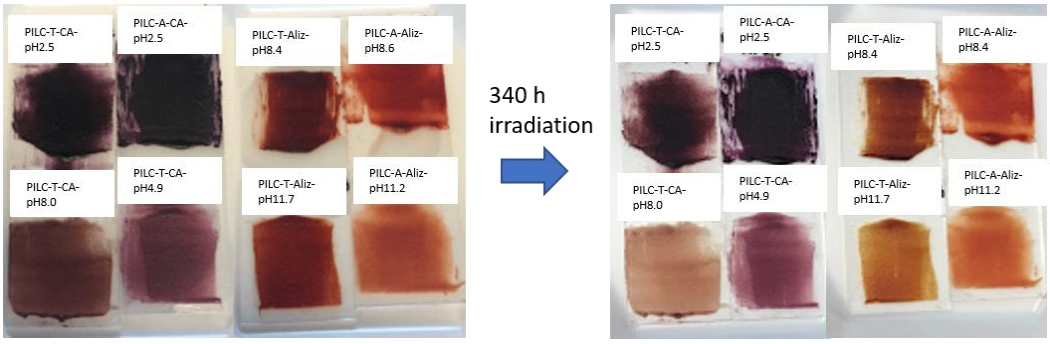

Figure 10(b). Oil paint formulations unexposed and exposed LED irradiation. Hybrid pigments based Aliz and CA organic dyes onto pillared clays.

The spectral reflectance distribution curve of hybrid pigments, before and after photoaging test, are shown in Figure 11 and 12. In general, all samples present similar spectra. The differences are observed for PILC-Ti-CA-pH2.5 and PILC-Ti-Aliz-pH8.4 solid pigment where after light exposure, a shift at higher values of reflectance is observed. It is probably due to the degradation/fading of the dye as observed in Figure 11. Oil painting samples had lower reflectance values compared to the solid pigments and all samples present very similar reflectance spectrum, according to Figure 12, suggesting less variation of colors consequently high resistance of the formulations even after a long time of irradiation.

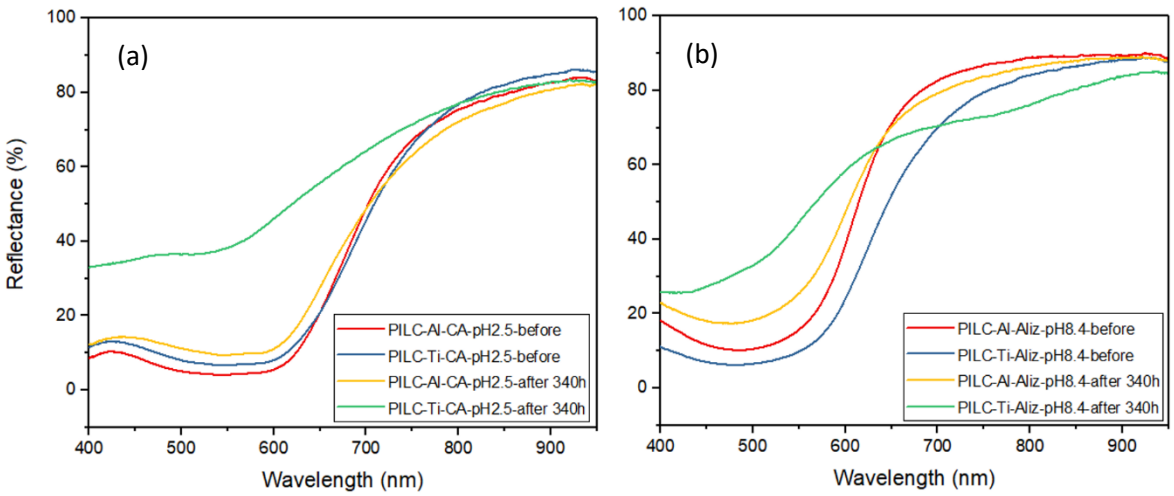

Figure 11. Reflectance spectrum of solid pigments before and after light exposure for 340 h for (a) carminic acid and (b) alizarin dyed samples.

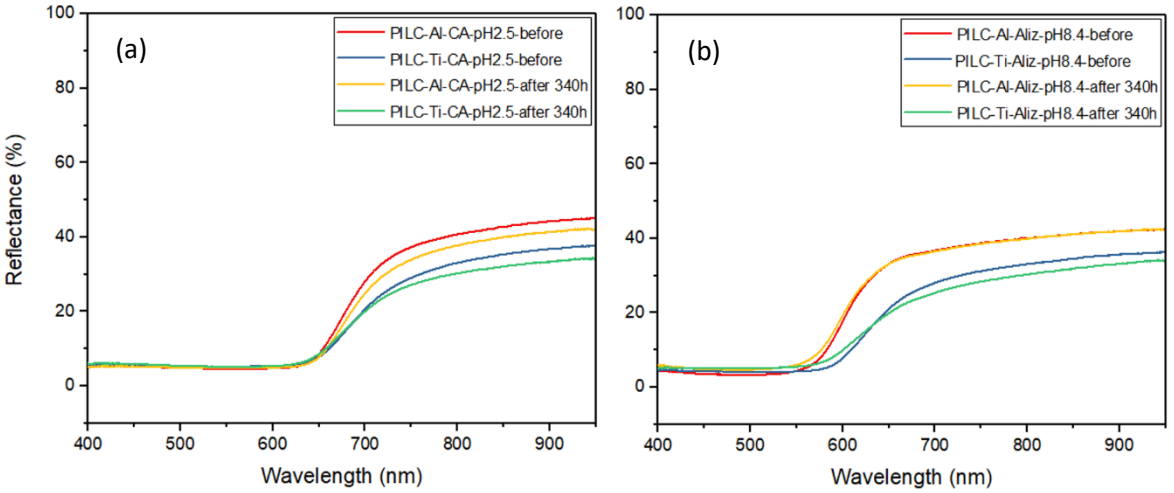

Figure 12. Reflectance spectra of oil paintings formulation before and after light exposure for 340 h for (a) CA and (b) Aliz dyed samples.

The measurement over CIE L^*, a^* and b^* scales notices a quantitative change over the pigments. ΔE^* variation values are due to the change of pigment structure after light exposure. Higher values of ΔE^* are observed for solid pigments (Figure 13a). Indeed, $\Delta E^*<14$ for dyes adsorbed on PILC-Al samples and $\Delta E^*<36$ for dyes adsorbed in PILC-Ti clays are noticed. Al-pillared based pigments have been shown more stable than Ti-pillared based. This may probably due to the photocatalytic property of the anatase phase that remains even after the

complexation of the pillared material with the dye molecule. In all samples, lower values of ΔE^* are observed for oil paint formulations, mainly aluminium based samples (Figure 13b). These results suggested high stability of the ink formulations upon incorporation of drying oil, probably the linseed oil in the surface of the pigment, disturbs the reactions with oxygen. When irradiation is performed in air, the clay will have much faster access to new oxygen coming from outside which would result in higher dye photobleaching rates at that region [45] because the oxygen seems to play a key role for the dye photostability. Linseed oil can be acting as an inhibitor in the formation of the radicals, forming a photoresist protective layer.

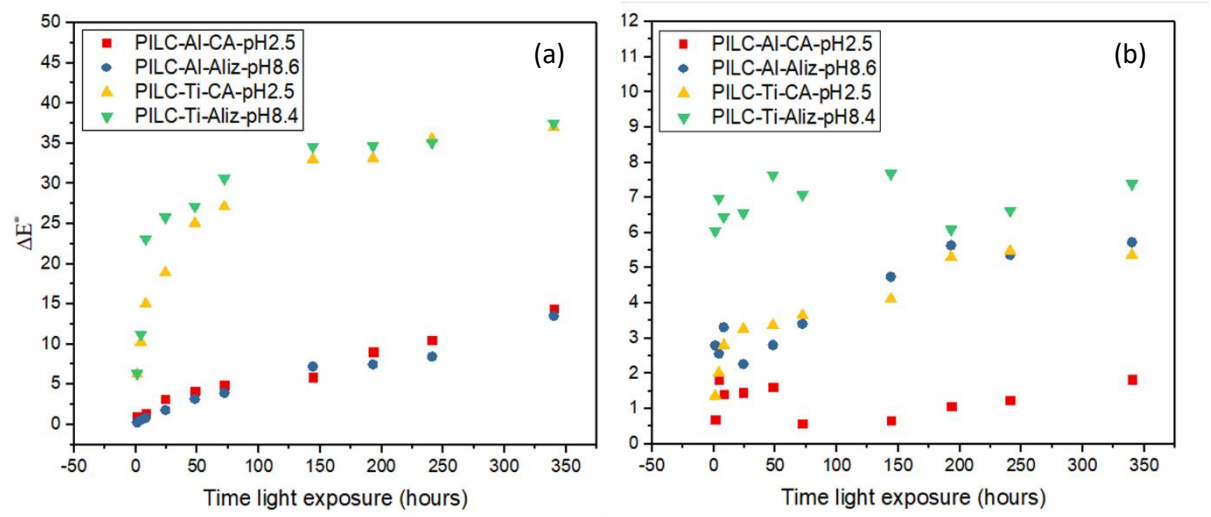

Figure 13. Colour difference (ΔE^*) between (a) solid pigments and (b) oil painting formulation samples exposed to the light-induced aging for 340 h.

According to these results, after light exposure, fading occurs in the solid pigments, especially in samples pillarized with titanium cations. Aluminum-based samples are more stable due to the strong interactions between the dye molecules and the modified clay, that retard photodegradation. The painting formulations exhibit minor variations in the L^*, a^* and b^* parameters after a long period of exposure to light, perhaps the formulations inhibit the hydroperoxides formation that accelerate the photo-oxidation process [46].

5.0 CONCLUSIONS

Hybrid pigments were prepared by stabilization of organic dyes onto pillared montmorillonite. XDR, TEM and BET analyses suggest that pillaring process occurs. The interactions between chromophore groups and clay surface is driven by electrostatic forces and/or complexation between metallic cations in the interlamellar space and ketone and hydroxyl functions in the dye molecule. These results were highlighted by Infrared and NMR experiments. Fluorescence analysis report that increase of average lifetime for dyes upon adsorption on modified clay confirm interactions between organic dyes and clay mineral and underline the strong dependence on the speciation. Different parameters influence the color and hue of the hybrids the pH, the amount of the adsorbed dyes and the nature of metallic cations in the interlayer space. Oil paint formulations simulate real materials used in paintings. High stability of the organic-inorganic hybrids, especially from aluminium pillared clays dyed with carminic acid and alizarin, indicate that these can be applied as new stable lake pigments.

6.0 ACKNOWLEDGEMENTS

We acknowledge the financial support from the CAPES/COFEBUB (Project n° 835/15). The authors thank the Île-de-France region and CNRS for funding.

7.0 REFERENCES

[1] Fournier F, de Viguerie L, Balme S, Janot JM, Walter P, Jaber M. Physico-chemical

characterization of lake pigments based on montmorillonite and carminic acid. Applied Clay Science 2015;130:12–7.

[2] Bechtold T and Mussak R. Handbook of Natural Colorants 2009, Wiley, United Kingdon.

[3] Tian G, Wang W, Wang D, Wang Q, Wang A. Novel environment friendly inorganic red pigments based on attapulgite. Powder Technology 2017;315:60–7.

[4] Cao L, Fei X, Zhao H. Dyes and Pigments Environmental substitution for PbCrO 4 pigment with inorganic-organic hybrid pigment. Dyes and Pigments 2017;142:100–7.

[5] Pereira F, Sousa K, Cavalcanti G, França D, Queiroga L, Santos I, Fonseca M, Jaber M. Green biosorbents based on chitosan-montmorillonite beads for anionic dye removal. Journal of Environmental Chemical Engineering 2017;5:3309–18.

[6] Thangaraj V, Bussiere J, Janot JM, Bechelany M, Jaber M, Subramanian S, et al. Fluorescence Quenching of Sulforhodamine Dye over Graphene Oxide and Boron Nitride Nanosheets. European of Journal Inorganic Chemistry 2016;2016:2125–30.

[7] Zhang A, Mu B, Luo Z, Wang A. Dyes and Pigments Bright blue halloysite / CoAl 2 O 4 hybrid pigments : Preparation , characterization and application in water-based painting. Dyes and Pigments 2017;139:473–81.

[8] Pérez E, Ibarra IA, Guzmán A, Lima E. Hybrid pigments resulting from several guest dyes onto γ-alumina host: A spectroscopic analysis. Spectrochimica Acta Part A Mol ecular and Biomolecular Spectroscopy 2017;172:174–81.

[9] Claro A, Melo MJ, Schäfer S, de Melo JSS, Pina F, van den Berg KJ, et al. The use of microspectrofluorimetry for the characterization of lake pigments. Talanta

2008;74:922–9.

[10] Perez-Ramirez E, Lima E, Guzman A. Natural betalains supported on γ -alumina: A wide family of stable pigments. Dyes and Pigments 2015;120:161–8.

[11] Anselmi C, Capitani D, Tintaru A, Doherty B, Sgamellotti A, Miliani C. Beyond the color : A structural insight to eosin-based lakes. Dyes and Pigments 2017;140:297–311.

[12] Mintova S, Jaber M, Valtchev V. Nanosized microporous crystals: emerging applications. Chemical Society Reviews 2015;44:7207–33.

[13] El Adraa K, Georgelin T, Lambert JF, Jaber F, Tielens F, Jaber M. Cysteine-montmorillonite composites for heavy metal cation complexation: A combined experimental and theoretical study. Chemical Engineering Journal 2017;314:406–17.

[14] Arnold, D.E. Maya Blue and Palygorskite: A second possible pre-Columbian source. Ancient Mesoamerica 2005, 16, 51–62.

[15] Cocoletzi GH, Canto G. Trapping and diffusion of organic dyes inside of palygorskite clay : The ancient Maya Blue pigment. Microporous and Mesoporous Materials 2017;249.

[16] Wu S, Duan Z, Hao F, Xiong S, Xiong W, Lv Y, et al. Preparation of acid-activated sepiolite / Rhodamine B @ SiO 2 hybrid fl uorescent pigments with high stability. Dyes and Pigments 2017;137:395–402.

[17] Tian, G., Wang, W., Mu, B., Wang, Q., Wang, A., 2017a. Cost-efficient, vivid and stable red hybrid pigments derived from naturally available sepiolite and halloysite. Ceramics International 43, 1862–1869.

[18] Kittinaovarat S, Kansomwan P, Jiratumnukul N. Chitosan / modified montmorillonite

beads and adsorption Reactive Red 120. Applied Clay Science 2010;48:87–91.

[19] Jaber, M., Georgelin, T., Bazzi, H., Costa-torro, F., Clodic, G., 2014. Selectivities in adsorption and peptidic condensation in the (arginine and glutamic acid)/montmorillonite clay system. Journal of Physical Chemistry C 118, 44, 25447-25455

[20] Gil A, Assis FCC, Albeniz S, Korili SA. Removal of dyes from wastewaters by adsorption on pillared clays. Chemical Engineering Journal 2011;168:1032–40.

[21] Gil A, Gandía LM, Vicente MA. Recent Advances in the Synthesis and Catalytic Applications of Pillared Clays. Catalysis Reviews, 2017;4940.

[22] Li K, Lei J, Yuan G, Weerachanchai P, Wang JY, Zhao J, et al. Fe-, Ti-, Zr- and Al-pillared clays for efficient catalytic pyrolysis of mixed plastics. Chemical Engineering Journal 2017;317:800–9.

[23] Tangaraj V, Janot J, Jaber M, Bechelany M, Balme S. Adsorption and photophysical properties of fluorescent dyes over montmorillonite and saponite modified by surfactant. Chemosphere 2017, 184 1355-1361.

[24] Bergaoui L, Lambert J-F, Suquet H, Che M. CuII on Al13-Pillared Saponites: Macroscopic Adsorption Measurements and EPR Spectra. Journal of Physical Chemistry. 1995;99:2155–61.

[25] Tomul F, Turgut Basoglu F, Canbay H. Determination of adsorptive and catalytic properties of copper, silver and iron contain titanium-pillared bentonite for the removal bisphenol A from aqueous solution. Applied Surface Science 2016;360:579–93.

[26] MacHatova, Z., Barbierikova, Z., Poliak, P., Jancovicova, V., Lukes, V., Brezova, V., 2016. Study of natural anthraquinone colorants by EPR and UV/vis spectroscopy. Dyes

and Pigments 132, 79–93

[27] Miliani, C., Romani, a, Favaro, G., 2000. Acidichromic effects in 1, 2-di-and 1, 2, 4-trihydroxyanthraquinones. A spectrophotometric and fluorimetric study. Journal of Physical Organic Chemistry 141–150.

[28] Vágvölgyi V, Kovács J, Horváth E, Kristóf J, Makó É. Investigation of mechanochemically modified kaolinite surfaces by thermoanalytical and spectroscopic methods. Journal of Colloids and Interface Science 2008;317:523–9.

[29] Balme S, Guégan R, Janot J-M, Jaber M, Lepoitevin M, Dejardin P, et al. Structure, orientation and stability of lysozyme confined in layered materials. Soft Matter 2013;9:3188.

[30] Cornu, D., Lin, L., Daou, M.M., Jaber, M., Krafft, J.-M., Herledan, V., Laugel, G., Millot, Y., Lauron-Pernot, H., 2017. Influence of acid–base properties of Mg-based catalysts on transesterification: role of magnesium silicate hydrate formation. Catalisis Science Technology 7, 1701–1712.

[31] Ksontini N, Ã WN, Ghorbel A. Al – Fe pillared clays : Synthesis , characterization and catalytic wet air oxidation activity. Journal of Physics and Chemistry of Solids 2008;69:1112–5.

[32] Kumararaja P, Manjaiah KM, Datta SC, Sarkar B. Remediation of metal contaminated soil by aluminium pillared bentonite : Synthesis , characterisation , equilibrium study and plant growth experiment. Applied Clay Science 2017;137:115–22.

[33] Ooka C, Akita S, Ohashi Y, Horiuchi T, Suzuki K, Komai S, et al. Crystallization of hydrothermally treated TiO 2 pillars in pillared montmorillonite for improvement of the photocatalytic activity. Journal of Materials Chemistry 1999:2943–52.

[34] Barama S, Davidson A, Barama A, Boukhlouf H, Casale S, Calers C, et al. Dephosphatation under UV light of water by Ti-PILC with activation by secondary species (La, Se, and Rb). Comptes Rendus Chimie 2017;20:7–19.

[35] Liang X, Qi F, Liu P, Wei G, Su X, Ma L, et al. Performance of Ti-pillared montmorillonite supported Fe catalysts for toluene oxidation: The effect of Fe on catalytic activity. Applied Clay Science, 2016;132–133:96–104.

[36] Chmielarz L, Piwowarska Z, Kuśtrowski P, Wegrzyn A, Gil B, Kowalczyk A, et al. Comparison study of titania pillared interlayered clays and porous clay heterostructures modified with copper and iron as catalysts of the DeNOx process. Applied Clay Science, 2011;53:164–73.

[37] Bergaoui L, Lambert JF, Vicente-Rodriguez MA, Michot LJ, Villiéras F. Porosity of Synthetic Saponites with Variable Layer Charge Pillared by Al-13 Polycations. Langmuir, 1995;11:2840–52.

[38] Hutson ND, Hoekstra MJ, Yang RT. Control of microporosity of Al O -pillared clays : effect of pH , calcination temperature and clay cation exchange capacity. Microporous and Mesoporous Materials, 80, 1999;28:447–59.

[39] Roca Jalil ME, Baschini M, Rodríguez-Castellón E, Infantes-Molina A, Sapag K. Effect of the Al/clay ratio on the thiabendazol removal by aluminum pillared clays. Applied Clay Science 2014;87:245–53.

[40] Giustetto R, Wahyudi O, Corazzari I, Turci F. Applied Clay Science Chemical stability and dehydration behavior of a sepiolite / indigo Maya Blue pigment. Applied Clay Science, 2011;52:41–50.

[41] Doskocz M, Kubas K, Frackowiak A, Gancarz R. NMR and ab initio studies of Mg2+,

Ca2+, Zn2+, Cu2+ alizarin complexes. Polyhedron 2009;28:2201–5.

[42] Fain, V.Y., Zaitsev, B.E., Ryabov, M. a, 2004. Metal Complexes with 1 , 5- and Electronic Absorption Spectra and Structure of Ligands, Russian Journal of Coordination Chemistry 30, 385–389.

[43] Epstein M, Yariv S. Visible-spectroscopy study of the adsorption of alizarinate by Al-montmorillonite in aqueous suspensions and in solid state. Journal of Colloids Interface Science, 2003;263:377–85.

[44] Feng W, Nansheng D, Helin H. Degradation mechanism of azo dye C. I. reactive red 2 by iron powder reduction and photooxidation in aqueous solutions. Chemosphere 2000;41:1233–8.

[45] Lencione D, Gehlen MH, Trujillo LN, Leitao RCF, Albuquerque RQ. The spatial distribution of the photostability of thionine in zeolite L nanochannels investigated by Photobleaching Lifetime Imaging Microscopy. Photochemical and Photobiology Science, 2016;15:398–404.

[46] Wu T, Liu G, Zhao J, Hidaka H, Serpone N. Evidence for H2O2 Generation during the TiO2-Assisted Photodegradation of Dyes in Aqueous Dispersions under Visible Light Illumination. Journal of Physical Chemistry B 1999;103:4862–7.